Gossamer bulk high-temperature superconductivity in FeSe

A.A. Sinchenko[1,2],P.D. Grigoriev[3,4,5*], A.P. Orlov[1], A.V. Frolov[1],
A. Shakin[5], D.A. Chareev[6,7], O.S. Volkova[5,6,8] and A.N. Vasiliev[5,6,8]
[1]*Kotelnikov Institute of Radioengineering and Electronics of RAS, Mokhovaya 11-7, 125009 Moscow, Russia*
[2]*National Research Nuclear University (MEPhI), 115409 Moscow,Russia*
[3]*L.D. Landau Institute for Theoretical Physics, 142432 Chernogolovka, Russia**
[4]*P.N. Lebedev Physical Institute, RAS, 119991, Moscow, Russia*
[5]*National University of Science and Technology "MISiS", 119049 Moscow, Russia*
[6]*Ural Federal University, 620002 Ekaterinburg, Russia*
[7]*Institute of Experimental Mineralogy, RAS, 142432 Chernogolovka, Russia and*
[8]*M.V. Lomonosov Moscow State University, 119991 Moscow, Russia*

The cuprates and iron-based high-temperature superconductors share many common features: layered strongly anisotropic crystal structure, strong electronic correlations, interplay between different types of electronic ordering, the intrinsic spatial inhomogeneity due to doping. The understanding of complex interplay between these factors is crucial for a directed search of new high-temperature superconductors. Here we show the appearance of inhomogeneous gossamer superconductivity in bulk FeSe compound at ambient pressure and at temperature 5 times higher than its zero-resistance T_c. This discovery helps to understand numerous remarkable superconducting properties of FeSe. We also find and prove a general property: if inhomogeneous superconductivity in a anisotropic conductor first appears in the form of isolated superconducting islands, it reduces electric resistivity anisotropically with maximal effect along the least conducting axis. This gives a simple and very general tool to detect inhomogeneous superconductivity in anisotropic compounds, which is critically important to study the onset of high-temperature superconductivity.

Introduction

A deep understanding of the mechanisms and prerequisites of high-temperature superconductivity is a fundamental challenge to condensed-matter physics. In spite of three-decade extensive research, the advance in this field is still insufficient to reliably predict new high-temperature superconductors. The maximal superconducting transition temperature T_c in the most promising cuprates and iron-based high-temperature superconductors appears at some non-stoichiometric chemical composition, or doping[1,2]. This inevitably leads to a spatial inhomogeneity of these compounds because of local variations of doping level. Hence, high-temperature superconductivity in these compounds, probably, first appears in the form of small isolated superconducting islands, which become connected and coherent with decreasing temperature or with changing another driving parameter, i.e. doping or pressure[3]. Such inhomogeneous superconductivity with disrupted long-range order is often called as *gossamer superconductivity*, the term first introduced by Robert Laughlin[4]. Transition to this specific state is supported by the diamagnetic response, observed in various cuprate superconductors far above T_c.[5–8] The numerous direct observation of inhomogeneous electronic structure on a microscopic scale of few nanometers using STM and other experimental tools was reported in $Bi_2Sr_2CaCu_2O_{8+\delta}$,[9–12] in $HgBa_2CuO_{4+\delta}$,[13] in Fe-based high-Tc superconductor Pr-doped $CaFe_2As_2$ ($T_c \approx 45$ K),[14] etc. The superconductivity in these compounds, probably, develops in two stages: (i) the preformation of Cooper pairs on isolated islands, which leads to the diamagnetic response and was even proposed to be an origin of pseudogap in cuprates,[3] and (ii) the onset of long-range coherence between superconducting islands, leading to a zero resistance along the whole sample.

Whether the spatial inhomogeneity is a concomitant or assistant feature of high-temperature superconductivity is still debated, although various theoretical models propose an enhancement of superconducting transition temperature due to such inhomogeneity.[3,15] It may also play an important role in thin FeSe films on the interface of $SrTiO_3$, where superconductivity with high transition temperature $T_c \sim 109K$ was reported[16]. In any case, it is highly desirable to have a general and simple experimental test if superconductivity first appears in the form of isolated islands. Such a test would be useful in high-T_c superconductors and in many other compounds. The spatial inhomogeneity of superconductivity may arise not only due to doping, but also due to an interplay between different types of electronic ordering. For example, the interplay between spin-density wave at imperfect Fermi-surface nesting and superconductivity in the organic superconductor $(TMTSF)_2PF_6$ also leads to inhomogeneous superconductivity and even to the anisotropic superconductivity onset: superconductivity in this layered compound first observed along the least conducting axis, perpendicular to conducting planes.[17,18] This feature looks odd and counterintuitive, however, the similar effect was also reported in another organic superconductor $(TMTSF)_2ClO_4$,[19] and in the cuprate high-Tc

superconductor $YBa_2Cu_4O_8$.[20]

In this paper we first formulate and prove a general property: if superconductivity in an anisotropic conductor appears in a gossamer form of disconnected superconducting islands, these islands reduce electric resistivity anisotropically, i.e. their influence is first seen in electron transport along least conducting axis, perpendicular to conducting planes. This property may show up as an anisotropic superconductivity onset: the electric resistivity drops considerably along least conducting axis and remain almost unchanged along conducting planes. Below we substantiate and describe this property theoretically, and then demonstrate it experimentally on a FeSe superconductor. Using this property we show that superconductivity in bulk FeSe at ambient pressure first appears in the form of isolated islands at temperature $T_c^* \approx 35 - 40K$, which is close to superconducting transition temperature at high pressure[21–23] and strongly exceeds the zero-resistance superconducting transition temperature $T_c = 8K$ at ambient pressure[24]. This discovery may help to understand numerous remarkable and unusual superconducting properties of this compound, e.g. the high transition temperature $T_c \sim 109K$ in thin FeSe films[16].

Theoretical description of resistivity drop due to rare superconducting islands

In a layered conductor with the anisotropy parameter $\eta \equiv \sigma_{zz}/\sigma_{xx} \ll 1$ and small superconducting islands of volume ratio $\phi \ll 1$ (see Fig. 1) there are two parallel ways for interlayer current j to flow, so that the total interlayer current and conductivity are approximately given by the sums of two terms: $j_{tot} = j_1 + j_2$ and $\sigma_{zz}^{tot} = \sigma_{zz}^{(1)} + \sigma_{zz}^{(2)}$. The first, standard way is with almost uniform current density and direction $\boldsymbol{j}_1(\boldsymbol{r})$ perpendicular to the conducting layers. The rare superconducting inclusions then only slightly increase corresponding interlayer conductivity $\sigma_{zz}^{(1)}$ proportionally to their volume ratio, and $\sigma_{zz}^{(1)} \sim \eta\sigma_{xx}$. The second way of interlayer current is via superconducting islands. Since these superconducting islands are rare, the major part of the current path is in the normal phase. But instead of flowing along the external field E_z, the current between the islands can flow along the highly conducting layers until it comes to another superconducting island which allows next lift in the interlayer direction. Then there is no local current density along the z-axis in the normal phase, and the interlayer conductivity $\sigma_{zz}^{(2)}$ does not acquire the small anisotropy factor η. However, its path along conducting layers between rare superconducting islands is long and inversely proportional to the volume ratio of superconducting phase ϕ, so that $\sigma_{zz}^{(2)} \sim \phi\sigma_{xx}$. Depending on the ratio η/ϕ the first or second way makes the main contribution to the interlayer conductivity σ_{zz}^{tot} in such a heterogeneous media.

In the limit of rare superconducting islands, when their volume fraction $\phi \ll 1$, one can apply the Maxwell's approximation (see Sec. 18.1.1 of Ref.[25]), first proposed by Maxwell in 1873 for isotropic 3D case. Then the isotropic 3D media of conductivity σ_1 with spherical inclusions (granules) of conductivity σ_2 with small volume fraction $\phi \ll 1$ is equivalent to the uniform media with effective conductivity σ_e determined by the linear equation (see Sec. A of Supplementary information for details)

$$\frac{\sigma_e - \sigma_1}{\sigma_e + 2\sigma_1} = \phi\frac{\sigma_2 - \sigma_1}{\sigma_2 + 2\sigma_1}, \tag{1}$$

which gives

$$\frac{\sigma_e}{\sigma_1} = 1 + \frac{3\phi\,(\sigma_2 - \sigma_1)}{\sigma_2\,(1-\phi) + \sigma_1\,(2+\phi)}. \tag{2}$$

The problem of conductivity in anisotropic media can be mapped to the problem of isotropic media with anisotropic coordinate dilations (see Sec. B of Supplementary information for details). Thus, the current flow in the media with the easy-plane anisotropy, i.e. where $\sigma_{zz} \ll \sigma_{xx} = \sigma_{yy}$, is similar to the current flow in (mapped) isotropic media with $\sigma_{zz}^* = \sigma_{xx}^* = \sigma_{yy}^* = \sigma_{xx}$ subjected to uniaxial dilation along the z-axis: $z_* = z/\sqrt{\eta}$, where $\eta = \sigma_{zz}/\sigma_{xx}$. Then the spherical inclusions inside anisotropic media transform to elongated ellipsoids with axis ratio $a_z/a_x = 1/\sqrt{\eta} \gg 1$ and eccentricity $\chi = \sqrt{1-\eta} \to 1$, which are similar to finite filaments along c-axis. The generalization of Eq. (1) for the mapped media is[25]

$$(1-\phi)\,(\boldsymbol{\sigma}_e^* - \sigma_1\boldsymbol{I}) + \frac{\phi\,(\boldsymbol{\sigma}_e^* - \sigma_2\boldsymbol{I})}{\boldsymbol{I} + \boldsymbol{A}\,(\sigma_2 - \sigma_1)/\sigma_1} = 0, \tag{3}$$

where $\boldsymbol{I}$ is a unitary 3x3 matrix, and the diagonal matrix $\boldsymbol{A}$ for prolate spheroidal ($a_x = a_y$) inclusions is

$$\boldsymbol{A} = \begin{pmatrix} Q & 0 & 0 \\ 0 & Q & 0 \\ 0 & 0 & 1-2Q \end{pmatrix}, \tag{4}$$

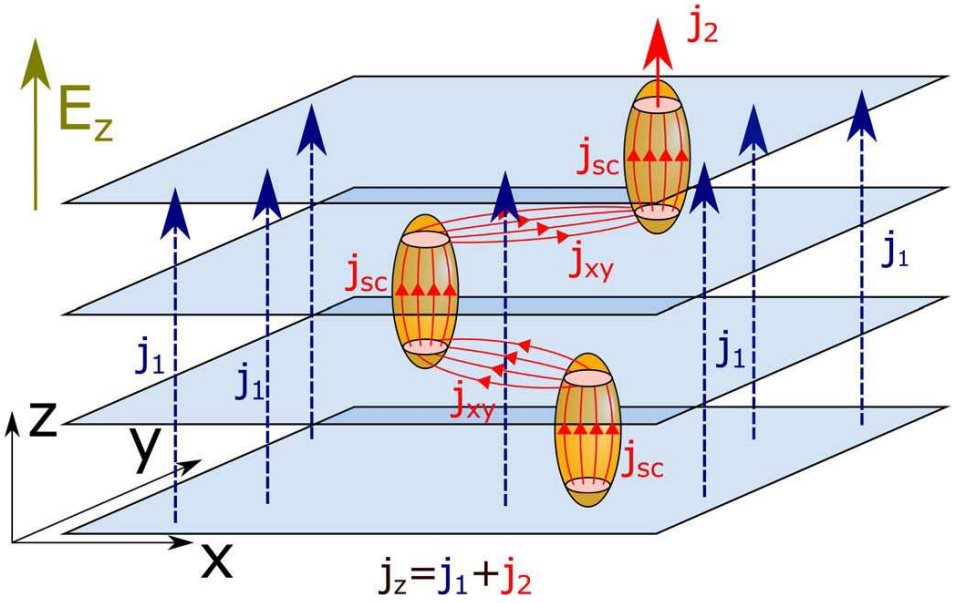

FIG. 1. **Illustration of two ways of interlayer current in a heterogeneous media with superconducting inclusions.** The first current path j_1, shown by blue arrows, is perpendicular to the conducting layers. The second diffusive path j_2, shown by red arrows, goes via superconducting islands and contains long intralayer tracks. The total interlayer current j_z is approximately a sum of these two contribution: $j_z \approx j_1 + j_2$. The yellow ellipsoids illustrate superconducting islands.

where

$$2Q = 1 + \frac{1}{1/\eta - 1}\left[1 - \frac{1}{2\chi}\ln\left(\frac{1+\chi}{1-\chi}\right)\right]. \tag{5}$$

For isotropic case $Q = 1/3$, the matrix $\boldsymbol{A} = \boldsymbol{I}/\boldsymbol{3}$, and Eq. (3) simplifies to Eq. (1). For strong anisotropy $\eta = \sigma_{zz}/\sigma_{xx} \ll 1$, the eccentricity $\chi \approx 1 - \eta/2$ is close to unity, and

$$Q \approx 1/2 + \eta\left[1 + \ln\left(\eta/4\right)/2\right]/2. \tag{6}$$

Substituting Eq. (4) to Eq. (3) gives the linear matrix equation on $\boldsymbol{\sigma}_e^*$:

$$(1-\phi)\left(\boldsymbol{\sigma}_e^* - \sigma_1\boldsymbol{I}\right)\left(\boldsymbol{I}\sigma_1 + \boldsymbol{A}\left(\sigma_2 - \sigma_1\right)\right) + \phi\left(\boldsymbol{\sigma}_e^* - \sigma_2\boldsymbol{I}\right)\sigma_1 = 0. \tag{7}$$

The solution of this equation is the diagonal matrix $\boldsymbol{\sigma}_e^*$. Its three diagonal elements at $\sigma_2/\sigma_1 \to \infty$ simplify to

$$\frac{\sigma_{xx}^*}{\sigma_1} \to \frac{Q\left(1-\phi\right)+\phi}{Q\left(1-\phi\right)} = 1 + \frac{\phi}{Q\left(1-\phi\right)}, \tag{8}$$

$\sigma_{yy}^* = \sigma_{xx}^*$, and

$$\frac{\sigma_{zz}^*}{\sigma_1} \to \frac{2Q\left(1-\phi\right)-1}{\left(2Q-1\right)\left(1-\phi\right)} = \frac{1}{1-\phi} + \frac{2Q\phi}{\left(1-2Q\right)\left(1-\phi\right)}. \tag{9}$$

For strongly anisotropic compounds with $\eta \ll 1$, substituting Eq. (6) and making reverse mapping $z = \sqrt{\eta}z_*$ and $\sigma_{zz} = \eta\sigma_{zz}^*$ to initial problem, from Eqs. (8) and (9) we finally obtain

$$\sigma_{xx} \approx \sigma_1\left(1 + 2\phi\right), \tag{10}$$

and

$$\sigma_{zz} \approx \sigma_1\left(\frac{\eta}{1-\phi} + \frac{\phi}{\ln\left(2/\sqrt{\eta}\right) - 1}\right). \tag{11}$$

The expression (11) for interlayer conductivity σ_{zz} consists of two parts. The first (regular) part at $\phi \ll 1$ only slightly increases, similarly to σ_{xx}. This part corresponds to the usual interlayer transport with local current density j_1 almost perpendicular to conducting layers, so that it contains the small anisotropy factor $\sigma_{zz}/\sigma_{xx} \approx \eta$. The second (irregular) part of σ_{zz} in Eq. (11) corresponds to the strongly nonuniform current density j_2: the current flows via superconducting islands along z-axis and between these superconducting islands along conducting (x, y) planes. This term does not have small anisotropy factor η, but contains another small factor ϕ, the volume fraction of superconducting islands. Hence, at $\phi > \eta$ the resulting conductivity anisotropy due to spherical superconducting islands reduces from $\sigma_{xx}/\sigma_{zz} = 1/\eta \gg 1$ to $\sigma_{xx}/\sigma_{zz} \approx 1/\phi$.

Methods

For present experiments we have chosen good quality plate-like single crystals (flakes) of $FeSe_{1-\delta}$ superconductor, grown in evacuated quartz ampoules using AlCl3/KCl flux technique in permanent temperature gradient, as described in[26]. Thin single-crystal samples with a thickness typically 2-4 μm were prepared by micromechanical exfoliation of relatively thick crystals. The structures of two types have been fabricated by the focused ion beam (FIB) technique described in[27] from selected samples (see Fig. 2 (a) and (b)). Structure of the first type, called below as A-type and shown in Fig.2a, is an in-plane bridge of length 20μm, width 2 μm, and thickness equal to single crystal thickness. This bridge is used to measure the intralayer resistance ρ_{ab}. Structure of the second type, shown in Fig.2b and called below as B-type, is a bridge oriented transverse to the layers, along the c-axis, with a typical sizes $L_a \times L_b \times L_c$ =2μm×2μm×0.2 μm. This bridge is used to measure the interlayer resistance ρ_c. The electrical contacts to the crystal have been prepared by the laser evaporation of gold films before the processing by FIB. The measurements of electrical resistance and of current-voltage (IV) characteristics have been done in the conventional 4-probe configuration. The temperature dependence of magnetic susceptibility of FeSe single crystal was obtained by AC Measurement option of Physical Property Measurement System – 9T Quantum Design. The plate was oriented perpendicular to external magnetic field $H = 10$ Oe applied at frequency 10 kHz. The demagnetizing factor $N \sim 0.5$ was supposed to obtain the full Meissner effect $4\pi\chi = -1$ for a finite size plate in accordance with classical formula[28].

Results and discussion

Fig.2 (c) shows the temperature dependence of resistivity in the structures of both types. The well-defined geometry of these structures allowed us to determine the conductivity anisotropy ratio ρ_c/ρ_{ab} and its temperature evolution, shown in Fig.2d. At room temperature $\rho_c/\rho_{ab} \approx 160 - 180$ and increases monotonically with temperature, reaching ≈ 500 at $T = 12$K. Note, that this increase of anisotropy goes in two stages. First, in the temperature range 300-90 K, the rate of this increase is about $0.25 - 0.30$ K^{-1}. Then, below 90 K, this rate increases by one order of magnitude, achieving 2.5-3.0 K^{-1}. Such a behavior reflects the strong decreasing of interlayer conductivity at temperature below the structural transition.[29,30] Additionally, in Fig. Fig.2d one may see a small kink at $T \approx 35K$. This feature is discussed below in detail. We suggest that it comes due to the appearance of inhomogeneous superconductivity in the form of isolated microscopic islands. Taking into account the layered crystal structure of FeSe, in B-type structures one may expect to observe some effects of weak superconductivity, namely, intrinsic Josephson effect, similar to that in layered cuprate high-T_c superconductors[31]. Surprisingly, in our structures we have observed just opposite picture: superconductivity is stronger in the direction perpendicular to conducting layers as compared to intralayer superconductivity. Inset in Fig.2c demonstrates superconducting transition for both types of structures. As can be seen, superconducting temperature in B-type structure is higher than in A-type structure. Such a behavior was observed for all studied samples. Moreover, the critical current density in the B-type structures is also larger by an order of magnitude.

Most interesting result was obtained during the study of the current-voltage (IV) characteristics of the bridge structures at temperature above T_c. Typical linear $R(T)$ behavior in a normal metallic state corresponds to the quadratic dependence of differential resistance on voltage because of the small Joule heating. In our case one may expect small deviations from this square dependence caused by superconducting fluctuations which appear in IV curves as excess conductivity at temperature close to T_c. Fig.3 (a) and (b) illustrates dV/dI as a function of V^2 at different temperatures above T_c for the A-type and B-type structures respectively. Figs. 3c and 3d show corresponding excess conductivity as a function of current, which was obtained by the extracting of normal state quadratic background from the experimental IV curves. One sees that the intralayer electronic transport in A-type structure demonstrates conventional for superconductors behavior: excess conductivity and, correspondingly, the superconducting fluctuations disappear rapidly above bulk T_c and they are absent completely above $T = 13$ K. This result correlates well with $R(T)$ behavior for this type structures (inset in Fig. 2c).

Quite different behaviour is observed in the interlayer electronic transport, i.e. in the B-type structure. As can be seen from Fig. 3(b,c), the excess conductivity is much more pronounced and, more importantly, observed up to $T \approx 35$

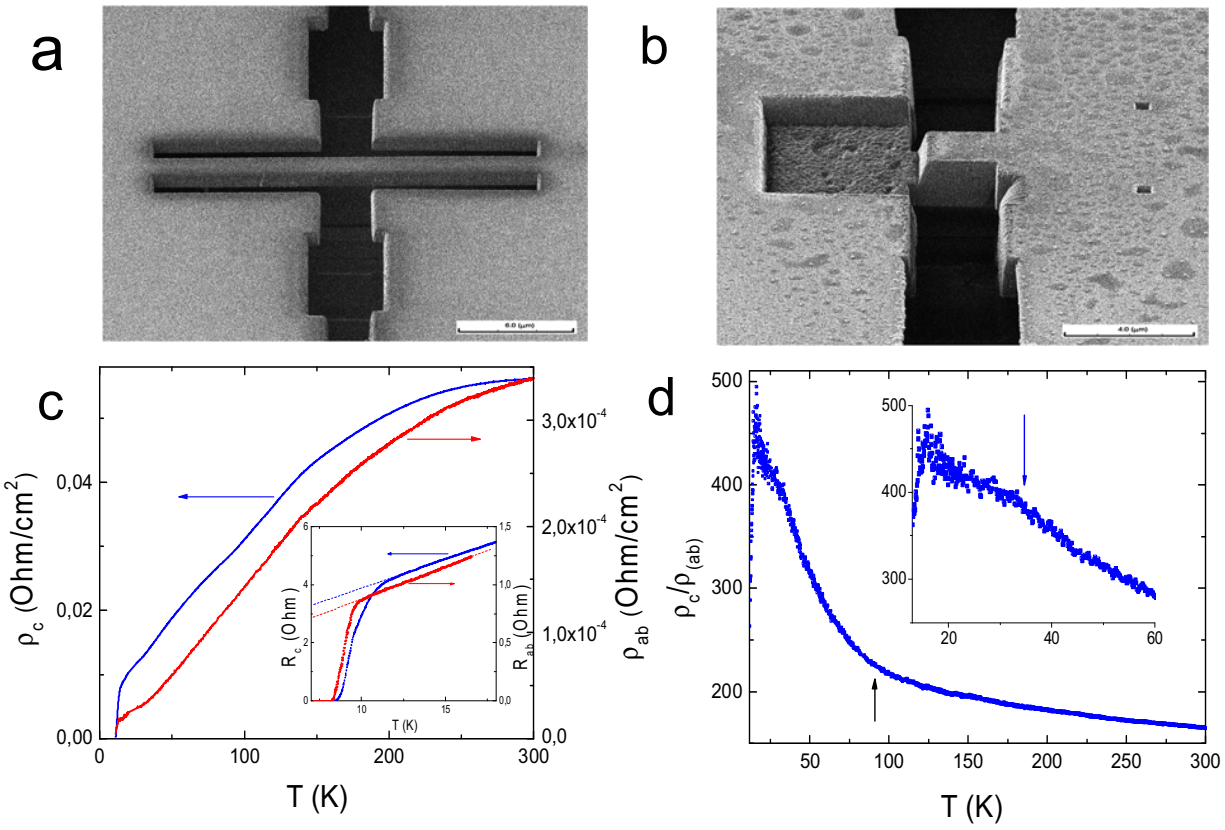

FIG. 2. **Intra- and interlayer conductivity measurements. a,** The SIM image of FeSe in-plane microbridge; **b,** The SIM image of FeSe microbridge (overlap structure) oriented along c-axis; **c,** temperature dependencies of resistivity: red curve – structure A and blue curve – structure B. Inset shows superconducting transition for both types of structures; **d,** Anisotropy of conductivity, ρ_c/ρ_{ab} as a function of temperature.

K. Note, that $R(T)$ for this type of junction is strongly linear at least in the temperature range 14-25 K (see inset in Fig.2c). It means, that simple fluctuation effects cannot cause the observed excess conductivity. The difference between intralayer and interlayer conductivity is clearly seen in Fig.3e, where we plot the temperature dependence of excess conductivity for both types of structures.

We see only one explanation of the observed effect: the formation of small superconducting islands with $T_c^* \approx 35-40$ K. Then at $T = T_c^*$ the corresponding decrease of resistance $R(T)$ should be anisotropic according to the above theoretical model.

Our results are in agreement with the recent work[32] where a rise in T_c more than twice was observed in point-contacts between FeSe single crystal and Cu. Actually, authors of this work observed some excess conductivity at temperature well above T_c. The point-contact was formed between cooper wire and the plane of FeSe crystal. It is well known that the point-contact itself is directional with respect to the electric-field configuration[33], and one may expect that the main contribution to the point-contact resistance comes from injection along the point-contact orientation, making point contact configuration close to our structures. Then the authors of Ref.[32] probed the electronic transport mainly along the c-axis and, therefore, observed similar effect from the filamentary gossamer superconductivity.

We observe small peculiarities already in the $R(T)$ dependencies which may indicate the appearance of superconducting islands. A very small but visible decrease of interlayer resistance can be noticed at $T \approx 42-45$ K as shown in Fig. 4(a). This effect is more pronounced in the derivative curve, $dR/dT(T)$, shown in the inset to Fig. 4(a). Note, that this feature is completely absent in the intralayer resistance. As one can see in the inset in Fig.2(d), at nearly the same temperature some decrease of anisotropy is also observed.

One of the best ways to detect the existence of small volume fraction of superconductivity is the measurement of magnetic susceptibility. In the present work we also measured the magnetic properties of studied crystals. The temperature dependence of the real part of magnetic susceptibility $4\pi\chi$ shown in Fig. 4 (b) demonstrates a negative deviation in the whole temperature range. At high temperatures it decreases almost linearly then bends down at approximately 50 K which can be seen more clearly in double logarithmic scale shown in the Inset to Fig. 4 (b),

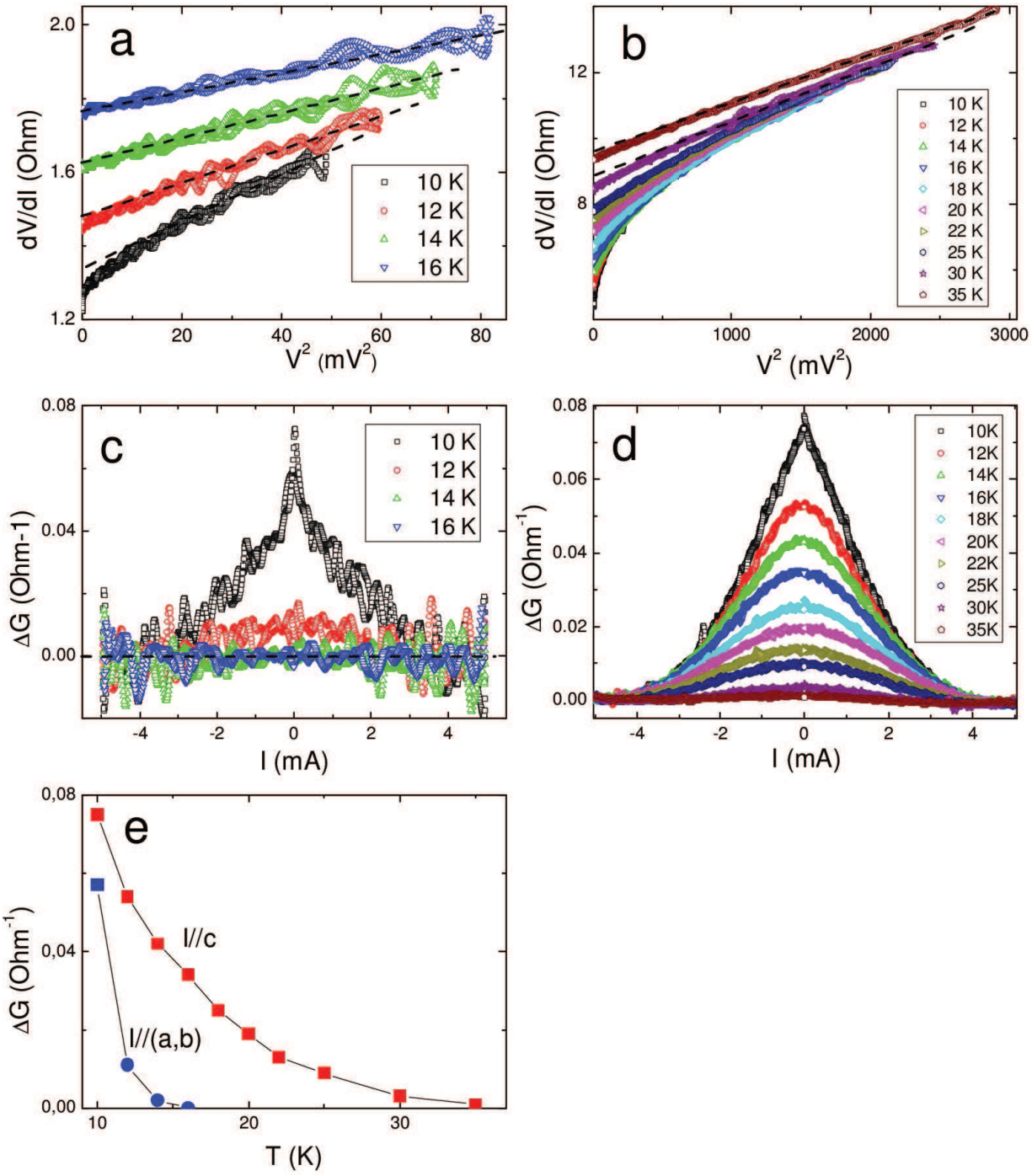

FIG. 3. **Excess conductivity for two perpendicular current directions. a,** Differential resistance dV/dI as a function of the square of voltage, V^2, at different temperatures above T_c for A-type structure, i.e. for intralayer transport. **b,** The same as (a) but for B-type structure, i.e. for interlayer transport. **c,** Excess differential conductivity as a function of current for A-type structure measured at different temperatures above T_c. **d,** The same as in (c) but for B-type structure. **e,** Temperature dependence of excess conductivity: red square symbols for the B-type structure, and blue circle symbols for the A-type structure.

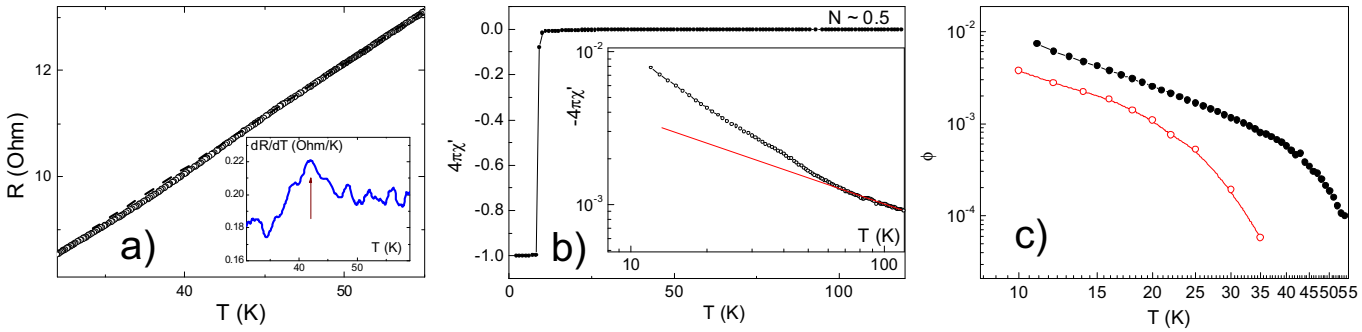

FIG. 4. **Temperature dependence of the volume fraction of superconducting islands. a,** Temperature dependence of interlayer resistance in the temperature range 30-60 K demonstrating small decrease of resistance at $T \approx 45$ K. Inset shows the derivative of this curve. **b,** The temperature dependence of real part of magnetic susceptibility of FeSe single crystal. Main panel contains initial $4\pi\chi$ curve obtained for demagnetizing factor $N \sim 0.5$, and the inset represents the same curve in double logarithmic scale to highlight the negative deviation at high temperatures. The line is a guide for an eye. **c,** The temperature dependence of superconducting volume fraction ϕ obtained from magnetic (closed circles) and from transport (open circles) measurements. In the latter case, the volume fraction ϕ of superconducting phase was calculated from equation (11).

and finally drops to absolute diamagnetic value $4\pi\chi = -1$ below superconducting phase transition $T_C = 9$ K. The rough estimation of superconducting phase portion ϕ can be done by subtraction of linear function from $4\pi\chi(T)$ dependence assuming 100% of superconducting phase at low temperatures $T \ll T_C$. The temperature dependencies of superconducting phase percentage obtained from magnetic (closed circles) and transport (open circles) measurements are shown in Fig. 4 (c). In the latter case, the volume fraction ϕ of superconducting phase was calculated from Eq. 11 using the experimental data on conductivity anisotropy, shown in Fig. 2d. Fig. 4(c) shows that ϕ is very small and decreases monotonically with increasing temperature. It is distinguishable below 50 K and amounts 10^{-4} at this temperature. At lower temperatures it is somewhat higher and comprises 10^{-2} above T_c. The shape of $\phi(T)$ dependence obtained from magnetic measurements is similar to that from transport measurements (see Fig. 4c).

Conclusions

In this paper we report the discovery of inhomogeneous superconductivity in bulk $FeSe_{1-\delta}$ at ambient pressure and at temperature $T_c^* \sim 35K$, which is 5 times higher than its zero-resistance superconducting transition temperature $T_c \approx 8K$ known before[24]. This superconductivity appears in the form of microscopic isolated superconducting islands and does not lead to zero electric resistance, but reveals itself in anisotropic resistivity drop and in magnetic susceptibility. Therefore, we called it gossamer inhomogeneous superconductivity. This discovery provides a clue to understand the nature of unusual superconducting properties of FeSe. For example, the pressure-temperature phase diagram of FeSe contains interplay between different electronic ordering and superconductivity with $T_c \sim 35K$ at pressure 6-8GPa,[21–23] which is the same as the transition temperature T_c^* of gossamer inhomogeneous superconductivity reported above. This coincidence is not occasional but suggests that the external pressure, by damping other types of electronic ordering, increases the volume fraction of superconducting regions, so that they become connected at pressure 6-8GPa. However, even at ambient pressure in FeSe there are microscopic superconducting islands without long-range coherence between these islands and, hence, without zero resistance.

Complementary, we proposed and described a general property: if inhomogeneous superconductivity in a anisotropic conductor first appears in the form of isolated superconducting islands, it reduces electric resistivity anisotropically with maximal effect along the least conducting axis. This property provides a simple and very general tool to detect inhomogeneous superconductivity in various anisotropic compounds. Namely, this method is applicable to almost all high-temperature superconductors, which have layered anisotropic crystal structure. The above study of FeSe is a nice illustration of this general tool. The anisotropic resistivity drop during the superconductivity onset was also reported in other layered superconductors, e.g. in organic superconductors $(TMTSF)_2PF_6$[17,18] and $(TMTSF)_2ClO_4$[19], and in even in the cuprate high-Tc superconductor $YBa_2Cu_4O_8$ (see Fig. 2 in Ref.[20]). Our model and Eq. (11) explains these observations and suggests inhomogeneous superconductivity onset also in these compounds. We believe that similar experimental test for inhomogeneous superconductivity can be performed in many other anisotropic superconductors, which will help to understand the mechanisms of high-temperature superconductivity.

Acknowledgements

P.G. thanks Dmitrii Lyubshin for useful discussion. This work was supported in part by the Ministry of Education and Science of the Russian Federation in the framework of Increase Competitiveness Program of NUST MISiS (# K2-2015-075, # K4-2015-020 and # K2-2016-003) and by Act 211 Government of the Russian Federation, contract # 02.A03.21.0006. Theoretical part was supported by RSCF # 16-42-01100.

Author contributions

A.A.S., A.O. and A.F. prepared the samples and performed the electronic transport measurements. P.G. proposed the theoretical description of the observed transport properties. O.V., A.S., D.Ch. and A.V. grew the crystals and performed the magnetic susceptibility measurements. All authors contributed to discussions.

---

* grigorev@itp.ac.ru

[1] Keimer, B., Kivelson, S. A., Norman, M. R., Uchida, S., & Zaanen, J., Nature **518**, 179 (2015).

[2] Si, Qimiao, Yu, Rong & Abrahams, Elihu, Nature Reviews Materials **1**, 16017 (2016); DOI:10.1038/natrevmats.2016.17.

[3] Kresin, V.Z., Ovchinnikov, Yu.N., & Wolf, S.A. Inhomogeneous superconductivity and the "pseudogap" state of novel superconductors, Physics Reports **431**, 231 – 259 (2006).

[4] Laughlin, R.B. Gossamer superconductivity, Philosophical Magazine, **86**, 1165–1171 (2006).

[5] Iguchi, I., Yamaguchi, T. & Sugimoto, A. Diamagnetic activity above Tc as a precursor to superconductivity in $La_{2-x}Sr_xCuO_4$ thin films, Nature **412**, 420-423 (2001).

[6] Bergemann, C., Tyler, A.W., Mackenzie, A.P., Cooper, J.R., Julian, S.R. & Farrell, D.E. Superconducting magnetization above the irreversibility line in $Tl_2Ba_2CuO_{6+\delta}$, Phys. Rev. B **57**, 14387–14396 (1998).

[7] Carretta, P., Lascialfari, A., Rigamonti, A., Rosso, A. & Varlamov, A. Superconducting fluctuations and anomalous diamagnetism in underdoped $YBa_2Cu_3O_{6+x}$ from magnetization and ^{63}Cu NMR-NQR relaxation measurements Phys. Rev. B 61, 12420–12426 (2000).

[8] Lascialfari, A. et al. Anomalous doping dependence of fluctuation-induced diamagnetism in $Y_{1-x}Ca_xBa_2Cu_3O_y$ superconductors, Phys. Rev. B **65**, 144523 (2002).

[9] S. H. Pan, S.H., et al. Microscopic electronic inhomogeneity in the high-Tc superconductor $Bi_2Sr_2CaCu_2O_{8+x}$. Nature **413**, 282–285 (2001).

[10] Lang, K. M. et al. Imaging the granular structure of high-TC superconductivity in underdoped $Bi_2Sr_2CaCu_2O_{8+\delta}$. Nature **415**, 412–416 (2002).

[11] Gomes, K.K., et al. Visualizing pair formation on the atomic scale in the high-Tc superconductor $Bi_2Sr_2CaCu_2O_{8+\delta}$. Nature **447**, 569–572 (2007).

[12] Wise, W.D. et al. Imaging nanoscale Fermi-surface variations in an inhomogeneous superconductor. Nature Physics **5**, 213–216 (2009).

[13] Campi, G., et al. Inhomogeneity of charge-density-wave order and quenched disorder in a high-Tc superconductor. Nature **525**, 359–362 (2015)

[14] Gofryk, K. et al. Local inhomogeneity and filamentary superconductivity in Pr-doped $CaFe_2As_2$. Phys. Rev. Lett. **112**, 047005 (2014).

[15] Martin, I., Podolsky, D & Kivelson, S.A. Enhancement of superconductivity by local inhomogeneities. Phys. Rev. B **72**, 060502(R) (2005).

[16] Jian-Feng Ge, J-F., et al. Superconductivity above 100 K in single-layer FeSe films on doped $SrTiO_3$. Nature Materials **14**, 285–289 (2015).

[17] N. Kang, et al. Domain walls at the spin-density-wave endpoint of the organic superconductor $(TMTSF)_2PF_6$ under pressure. Phys. Rev. B **81**, 100509(R)(2010).

[18] Narayanan, A., Kiswandhi, A., Graf, D., Brooks, J. & Chaikin, P. Coexistence of Spin Density Waves and Superconductivity in $(TMTSF)_2PF_6$. Phys. Rev. Lett. **112**, 146402 (2014).

[19] Ya. A. Gerasimenko, Ya.A., et al. Coexistence of superconductivity and spin-density wave in $(TMTSF)_2ClO_4$: Spatial structure of the two-phase state. Phys. Rev. B **89**, 054518 (2014).

[20] Hussey, N.E., Nozawa, K., Takagi, H., Adachi, S. & Tanabe, K. Anisotropic resistivity of YBa2Cu4O8: Incoherent-to-metallic crossover in the out-of-plane transport. Phys. Rev. B **56**, R11423–R11426 (1997).

[21] Mizuguchi, Y., Tomioka, F., Tsuda, S., Yamaguchi, T. & Takano, Y. Superconductivity at 27K in tetragonal FeSe under high pressure. Appl. Phys. Lett. **93**, 152505 (2008).

[22] Medvedev, S., et al. Electronic and magnetic phase diagram of β-$Fe_{1.01}Se$ with superconductivity at 36.7K under pressure. Nature Materials **8**, 630–633 (2009).

[23] J. P. Sun, J.P., et al. Dome-shaped magnetic order competing with high-temperature superconductivity at high pressures in FeSe. Nat. Commun. **7**, 12146 (2016).

[24] Hsu, F-C et al. Superconductivity in the PbO-type structure α-FeSe. PNAS **105**, 14262 (2008).

[25] Torquato, S. *Random Heterogeneous Materials*, Springer, 2001.

[26] Chareev, D., et al. Single crystal growth and characterization of tetragonal $FeSe_{1-x}$ superconductors. Cryst.Eng.Comm.

15(10), 1989–1993 (2013).
[27] Latyshev, Yu.I., et al. Interlayer tunnelling spectroscopy of the charge density wave state in $NbSe_3$. J. Phys. A: Math. Gen. **36**, 9323–9335 (2003).
[28] Goldfarb, R.B., Lelental, M. &Thompson, C.A. Alternating-field susceptometry and magnetic susceptibility of superconductors in *Magnetic susceptibility of superconductors and other spin systems* Ed. Hein R A, Francavilla T L and Liebenberg D H (New York : Plenum) pp 49-80 (1991).
[29] McQueen, T.M. et al. Tetragonal-to-Orthorhombic Structural Phase Transition at 90 K in the Superconductor $Fe_{1.01}Se$. Phys. Rev. Lett. **103**, 057002 (2009).
[30] Terashima, T., et al. Pressure-Induced Antiferromagnetic Transition and Phase Diagram in FeSe. J. Phys. Soc. Jpn. **84**, 063701 (2015).
[31] Kleiner, R. & Muller, P. Intrinsic Josephson effects in high-Tc superconductors. Phys. Rev. B **49**, 1327–1341 (1994).
[32] Naidyuk, Yu.G., Fuchs, G., Chareev, D.A. & Vasiliev, A.N. Doubling of the critical temperature of FeSe observed in point contacts. Phys. Rev. B **93**, 144515 (2016).
[33] Sinchenko, A.A. & Monceau, P. Charge-density-wave gaps of $NbSe_3$ measured by point-contact spectroscopy in different crystallographic orientations. Phys. Rev.**67**, 125117 (2003).

Supplementary Material to "**Gossamer bulk high-temperature superconductivity in FeSe**"

A. Derivation of the effective conductivity in the Maxwell's approximation for heterogeneous media with spherical granules

The effective conductivity σ_e of heterogeneous media, where small granules of conductivity σ_2 are embedded in a media of conductivity σ_1, can be easily derived in the effective-medium Maxwell's approximation (see §18.1.1 of Ref. [1]). In this approximation a heterogeneous media is replaced by a uniform media of effective conductivity σ_e such that their electric potentials at large distance are the same. In the Maxwell's approximation the interaction between rare small granules is neglected, and in the external uniform electric field $\boldsymbol{E}_0$ each small granule of radius R_i polarizes and acquires an additional electric dipole moment $\boldsymbol{d}_i$ proportional to its volume and to the strength of the field E_0:

$$\boldsymbol{d}_i = \beta_{12} \boldsymbol{E}_0 R_i^3, \tag{1}$$

where (see §17.1.1 of Ref. [1])

$$\beta_{12} = (\sigma_2 - \sigma_1) / (\sigma_2 + 2\sigma_1) \tag{2}$$

is the "polarizability" of a sphere. Each such dipole moments changes the electric potential outside the granule by

$$\Delta\varphi_i = \boldsymbol{d}_i \boldsymbol{r} / r^3, \tag{3}$$

so that the total change of electric potential far away from the sphere R_0, i.e. at $r \gg R_0$ is given by the sum of all granules inside inhomogeneous sphere of radius R_0:

$$\Delta\varphi_t = \sum_i \frac{\boldsymbol{d}_i (\boldsymbol{r} - \boldsymbol{r}_i)}{|\boldsymbol{r} - \boldsymbol{r}_i|^3} \approx \frac{\sigma_2 - \sigma_1}{\sigma_2 + 2\sigma_1} \frac{\phi R_0^3}{r^2} E_0. \tag{4}$$

On the other hand, a single isotropic sphere of the radius R_0 and conductivity σ_e inside a media of conductivity σ_1 in a uniform field E_0 creates an additional potential

$$\Delta\varphi_t = \frac{\sigma_e - \sigma_1}{\sigma_e + 2\sigma_1} \frac{R_0^3}{r^2} E_0. \tag{5}$$

Comparing Eqs. (4) and (5) gives

$$\frac{\sigma_e - \sigma_1}{\sigma_e + 2\sigma_1} = \phi \frac{\sigma_2 - \sigma_1}{\sigma_2 + 2\sigma_1}, \tag{6}$$

which coincides with Eq. (1) of the main text.

B. Mapping of conductivity problem in anisotropic media to isotropic

The electrostatic equation of continuity in Cartesian coordinates can be written as

$$-\boldsymbol{\nabla j} = \sigma_{xx} \frac{\partial^2 V}{\partial x^2} + \sigma_{yy} \frac{\partial^2 V}{\partial y^2} + \sigma_{zz} \frac{\partial^2 V}{\partial z^2} = 0. \tag{7}$$

By the change of coordinates

$$x_* = x,\ y_* = \sqrt{\sigma_{yy}/\sigma_{xx}}\, y,\ z_* = \sqrt{\sigma_{zz}/\sigma_{xx}}\, z \tag{8}$$

and by the simultaneous conductivity change $\sigma^*_{zz} = \sigma^*_{yy} = \sigma^*_{xx} = \sigma_{xx}$ it transforms to the electrostatic continuity equation for isotropic media:

$$-\boldsymbol{\nabla j} = \sigma_{xx} \left(\frac{\partial^2 V}{\partial x_*^2} + \frac{\partial^2 V}{\partial y_*^2} + \frac{\partial^2 V}{\partial z_*^2} \right) = 0. \tag{9}$$

Hence, the initial problem of conductivity in anisotropic media with some boundary conditions can be mapped to the conductivity problem in isotropic media with new boundary conditions, obtained from initial boundary conditions by the anisotropic dilatation in Eq. (8).

[1] Torquato, S. *Random Heterogeneous Materials*, Springer, 2001.